PHYSICAL REVIEW C VOLUME 50, NUMBER 2 AUGUST 1994

Excitation of giant resonances in the ^{40}Ca$(e,e'n)^{39}$Ca reaction

C. Takakuwa,* T. Saito, S. Suzuki,† and K. Takahisa‡
Laboratory of Nuclear Science, Tohoku University, Mikamine, Taihakuku, Sendai 982, Japan

T. Tohei and T. Nakagawa
Department of Physics, Tohoku University, Aramaki, Aobaku, Sendai 980, Japan

K. Abe
Department of Nuclear Engineering, Tohoku University, Aramaki, Aobaku, Sendai 980, Japan
(Received 27 December 1993)

Decay neutrons from the ^{40}Ca$(e,e'n)^{39}$Ca reaction were studied in the giant resonance region. The cross sections and angular distributions, separated for n_0 and n_1 decays, were obtained for excitation energies between 19 and 27 MeV, at the effective momentum transfer of 0.35 fm^{-1}. Legendre polynomial coefficients obtained from fitting the data are compared with those from the $(e,e'p)$ reaction. In the energy range 19–21 MeV, the interference coefficients b_1 and b_3 for the ground state transition are in agreement, but the noninterference coefficient b_2 is different. The different behavior of the angular distribution for protons and neutrons may suggest the interference of the decay from a $T=0$ quadrupole resonance and the $T=1$ giant dipole resonance. A similar tendency was also seen in comparing with the $(e,e'p_1)$ reaction. The Legendre polynomial coefficients for the n_0 decay in the $(e,e'n)$ reaction, transformed to the photon point, agree well with those of the (γ,n_0) reaction. The reduced total cross section is consistent between the $(e,e'n)$ and (γ,n) reactions, but the cross section for $(e,e'n_0)$ is larger than that of (γ,n_0) near the peak of the resonance. The values of the longitudinal-transverse interference term are close to zero in the present region, which is rather small compared with the value near the resonance of the $(e,e'p)$ reaction.

PACS number(s): 25.30.Dh, 24.30.Cz, 27.40.+z

I. INTRODUCTION

The giant resonances in ^{40}Ca have been studied by photoreactions, inclusive electron scattering, and inelastic hadron scattering. However, in photoreactions the low resolution inherent in the use of bremsstrahlung sources did not allow measurements of decays to specific residual states. Recently, coincidence electron-scattering experiments such as $(e,e'p)$ and $(e,e'n)$ have become possible by using high duty factor electron beams. Such experiments can provide new insights into decay mechanisms. In these experiments it is possible to study with high resolution not only ground-state transitions, but also transitions to excited states.

The coincidence $(e,e'x)$ cross section can be expressed in terms of four structure functions: pure longitudinal (W_L), pure transverse (W_T), longitudinal-transverse interference (W_{LT}), and transverse-transverse interference (W_{TT}) terms. For forward scattering, the longitudinal structure function (W_L) would be the dominant contribution to the cross section. W_L can be compared with the photonuclear cross section on the basis of Siegert theorem. The transverse contribution is evaluated from the longitudinal-transverse interference term (W_{LT}) since the longitudinal term dominates at forward angles.

In this paper we report on a study of the giant resonances in ^{40}Ca by measurements of angular distributions and cross sections of decay neutrons in the ^{40}Ca$(e,e'n)^{39}$Ca reaction. There are no published experimental data which can be compared directly with the present results. Previous papers on the $(e,e'n)$ reaction have been published on only three targets ^{208}Pb [1], ^{116}Sn [2], and ^{12}C [3]. However, the ^{40}Ca$(\gamma,n_0)^{39}$Ca reaction has been measured by Kellie *et al.* [4]. By comparison with an RPA calculation based on a Skyrme force [5], they showed evidence of isoscalar $E2$ strength below 27 MeV, and indicated that isovector $E2$ strength could be present around 30 MeV. The photonuclear data transformed from the present $(e,e'n)$ angular distributions are compared with these data.

In hadron scattering the charged-particle decay of the giant quadrupole resonance (GQR) and giant monopole resonance (GMR) in ^{40}Ca was studied by inelastic scattering of ^{3}He and α particles [6–12]. In recent measurements the isoscalar GQR strength was found to be 50% or less of the $E2$ energy weighted sum rule (EWSR) around $E_x = 18$ MeV [11]. Also about 23% of the isoscalar $E0$ EWSR has been found between 10.5 and 15.7 MeV excitation energy [12].

Recently the cross sections and the angular distribu-

*Present address: Toshiba Co., R&D Center, Kawasaki 210, Japan.
†Present address: Japan Atomic Energy Research Institute, Nakagun 319-11, Japan.
‡Present address: Research Center for Nuclear Physics, Osaka University, Ibaraki 567, Japan.

0556-2813/94/50(2)/845(13)/$06.00

tions for the reaction $^{40}\mathrm{Ca}(e,e'p_0)^{39}\mathrm{K}$ have been obtained in the energy range of 17.5 to 21 MeV by Tanaka *et al.* [13]. By deriving the longitudinal-transverse interference and the noninterference terms they show that the reaction $^{40}\mathrm{Ca}(e,e'p_0)$ is a sequential process, via excitation of the giant dipole resonance (GDR), and that the $T1/C1$ interference term is consistent with a GDR excitation with a dominant $1f_{7/2}1d_{5/2}^{-1}$ configuration. The calculated $(e,e'p_0)$ and $(e,e'n_0)$ angular distributions show the characteristic feature corresponding to interference between $T = 0$ and $T = 1$ resonant amplitudes as demonstrated in $^{16}\mathrm{O}$ [14]; i.e., the proton angular distribution is forward peaked, while the neutron angular distribution is backward peaked. Measurements for the $^{40}\mathrm{Ca}(e,e'n)^{39}\mathrm{Ca}$ reaction are useful to obtain information on the structure and reaction mechanism of giant resonances in $^{40}\mathrm{Ca}$ from comparison with data for the $^{40}\mathrm{Ca}(\gamma,n)^{39}\mathrm{Ca}$ and $^{40}\mathrm{Ca}(e,e'p)^{39}\mathrm{K}$ reactions, and RPA calculations.

II. EXPERIMENTAL PROCEDURE

The measurements were carried out using electrons from the 150 MeV Pulse-Stretcher Ring at Tohoku University [15]. A 95.2 mg/cm^2 self-supporting target of natural Ca was bombarded by the beam with an energy of 129 MeV. The duty factor was $\sim$ 80% with an average current of $\sim$ 40 nA. Scattered electrons from the target were momentum analyzed at $\theta_e = 30°$ by a double-focusing magnetic spectrometer [16], which has a solid angle of 2.9 msr, a momentum acceptance of 5%, and a momentum resolution of 0.05%. The detection system for the scattered electrons consisted of a vertical drift chamber and three layers of long plastic scintillation counters.

The neutron angular distributions were measured using seven neutron detectors consisting of NE213 liquid scintillators, where six detectors had a diameter of 18 cm by 10 cm depth and one detector had a 20 cm diameter by 10 cm depth. These were placed in the electron scattering plane at $\theta_n = 7°$, 34°, 64°, 93°, 155°, 184°, and 214°, where θ_n was measured from the momentum transfer direction (Fig. 1). The front of each detector was placed 75 cm from the center of the scattering chamber. The neutron energy was determined by the time-of-flight (TOF) method. As the target, spectrometer, and neutron detectors were located in the same room as the pulse-stretcher ring, the neutron detectors were shielded with lead, paraffin, and concrete. Lead collimators were placed in front of bismuth plates 4 cm thick to absorb scattered electrons and soft γ rays from the target, as shown in Fig. 2. Detail of the experimental apparatus has been described elsewhere [3]. The photon energy calibration for the neutron detectors was performed with $^{22}\mathrm{Na}$, $^{137}\mathrm{Cs}$, $^{60}\mathrm{Co}$, and Am-Be sources. The Compton edge of the $^{137}\mathrm{Cs}$ γ ray was set as the detection threshold.

Great care was taken in obtaining the relative efficiency for the seven neutron detectors. The efficiency of each detector for neutrons up to 8 MeV was different. As the relative detection efficiency for each detector was critical, it was determined experimentally. The known spectrum of neutrons from a $^{252}\mathrm{Cf}$ source was measured with the same geometry as the experiment. It was measured by the time of flight to a neutron detector relative to the disintegration time, determined from a small scintillator

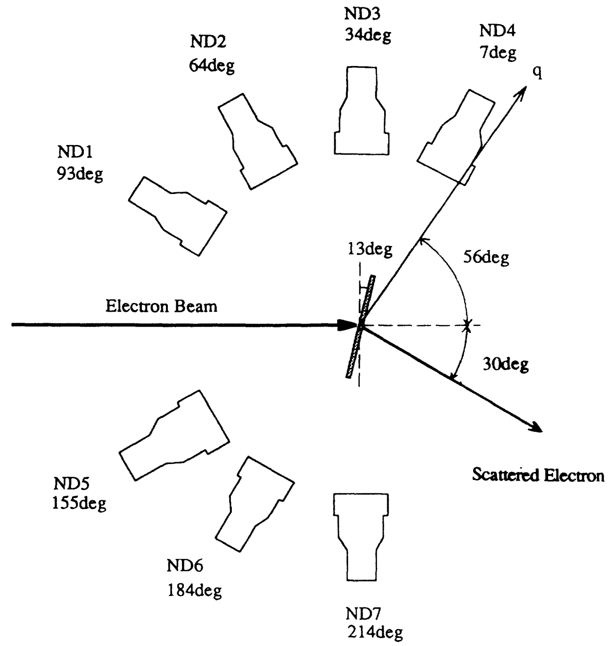

FIG. 1. Experimental arrangement. Each detector was placed 75 cm from the center of the scattering chamber. Detector angles are measured from the momentum transfer direction. An arrow indicated by q shows the direction of the momentum transfer.

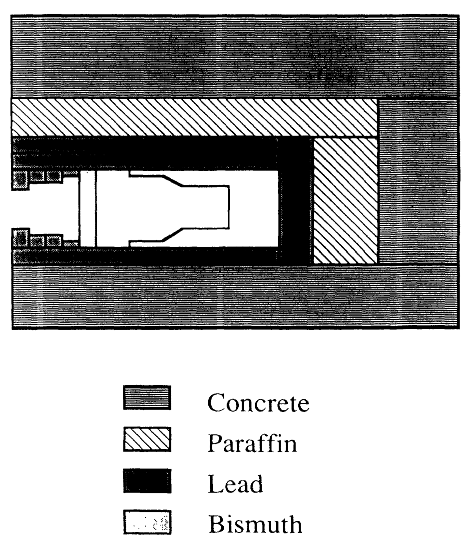

FIG. 2. Schematic view of the shielding for the neutron detectors.

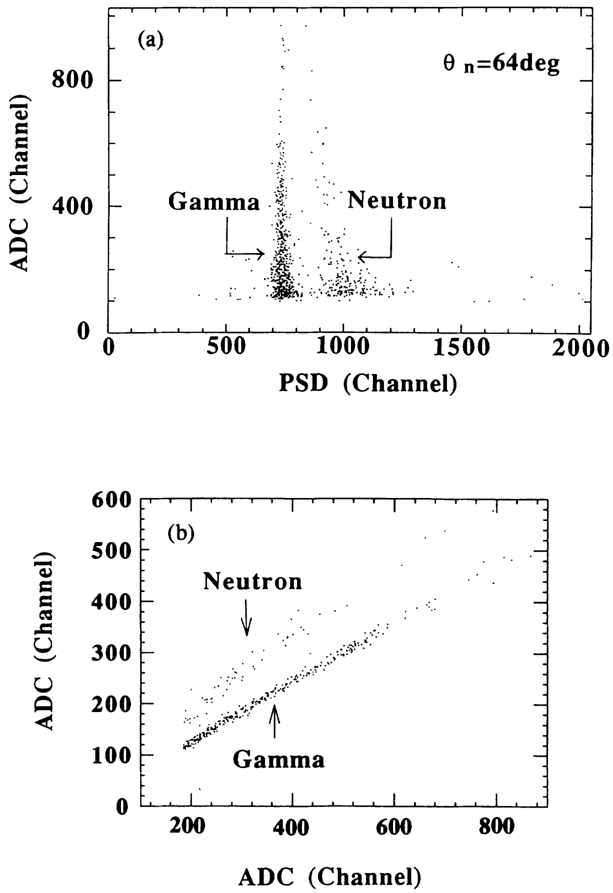

FIG. 3. (a) The two-dimensional plots of PSD-ADC signals from the neutron detector. (b) The two-dimensional plots of ADC-ADC signals from the neutron detector (charge comparison method).

placed near the ^{252}Cf source.

The effects of absorption by the bismuth, and rescattering of neutrons by the lead collimator were measured under similar experimental conditions. The counting rate increases $(0.8\pm0.15)\%$ because of the rescattering of neutrons, but there is no change in the detection efficiency as a function of neutron energies. The neutron attenuation factor for the bismuth absorber was $24.3 \pm 1.2\%$ for neutrons of energies 3–10 MeV. The absolute efficiency was obtained by normalizing the relative efficiency to the value calculated in the energy range 6–8 MeV by a Monte Carlo code [17]. The experimental detection efficiency was used for neutrons up to 8 MeV and the efficiency calculated by the Monte Carlo code was used for neutrons above 8 MeV.

NE213 scintillators respond to both γ rays and neutron events, but these events can be separated by pulse-shape discrimination (PSD). Two methods were used; a standard Canberra PSD unit and a charge comparison method. Figures 3(a) and 3(b) show the two-dimensional plots of PSD-ADC signals and n/γ separation obtained using the charge comparison method. It can be seen that neutrons are clearly separated from γ rays by both methods.

III. DATA ANALYSIS

A. Missing energy spectrum

The TOF spectrum obtained in the ^{40}Ca$(e,e'n)^{39}$Ca experiment after γ/n separation is shown in Fig. 4. This spectrum consists of true neutron and accidental neutron events. The true neutron events are obtained by subtracting the peak region from the corresponding background, estimated from the flat region. A missing energy E_m is calculated for each coincidence event using relation $E_m = \omega - E_n - E_R$, where ω is the excitation energy, E_n is the kinetic energy of the emitted neutron, and E_R is the recoil energy of the residual nucleus. The missing energy E_m corresponds to the excitation energy of the residual nucleus plus the binding energy. The missing energy spectrum for each detector is shown in Fig. 5; two peaks are clearly visible. From the spectra, the neutron energy resolution was found to be about 1.5 MeV at FWHM.

The peak at 15.6 MeV corresponds to the neutrons feeding the ground state in ^{39}Ca, the n_0 group. The peak at 17.8 MeV must correspond to the neutrons emitted to the first, second, and third excited states in ^{39}Ca; n_1, n_2, n_3. In the residual nucleus ^{39}Ca, the ground state differs by 2.467 MeV from the first excited state, but the first, second, and third excited states are closely spaced; so although we could separate the n_0 group, we could not separate n_1, n_2, and n_3. Hereafter n_1 stands for the summed quantities of n_1, n_2, and n_3.

B. Cross section

The ^{40}Ca$(e,e'n_0)^{39}$Ca and ^{40}Ca$(e,e'n_1)^{39}$Ca cross sections were obtained by summing the events within energy transfer (ω) intervals of 1.23 MeV for each peak in the missing energy spectrum. The results are shown in Figs. 6(a) and 6(b). The cross sections for $(e,e'n_0)$ and $(e,e'n_1)$ were not measured below excitation energies of 18.5 MeV and 21 MeV, respectively, because of the neutron detection threshold.

The theoretical $(e,e'x)$ cross sections can be expressed as [18,19]

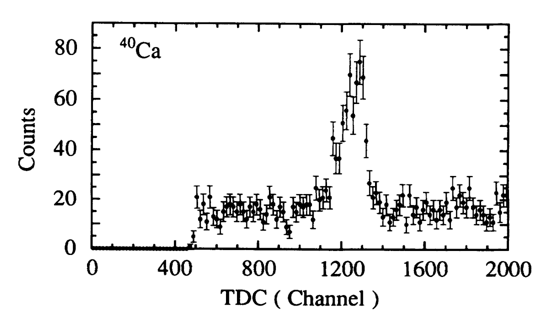

FIG. 4. Typical neutron time-of-flight spectrum. The peak is due to true events and counts in other area are accidental coincidence events.

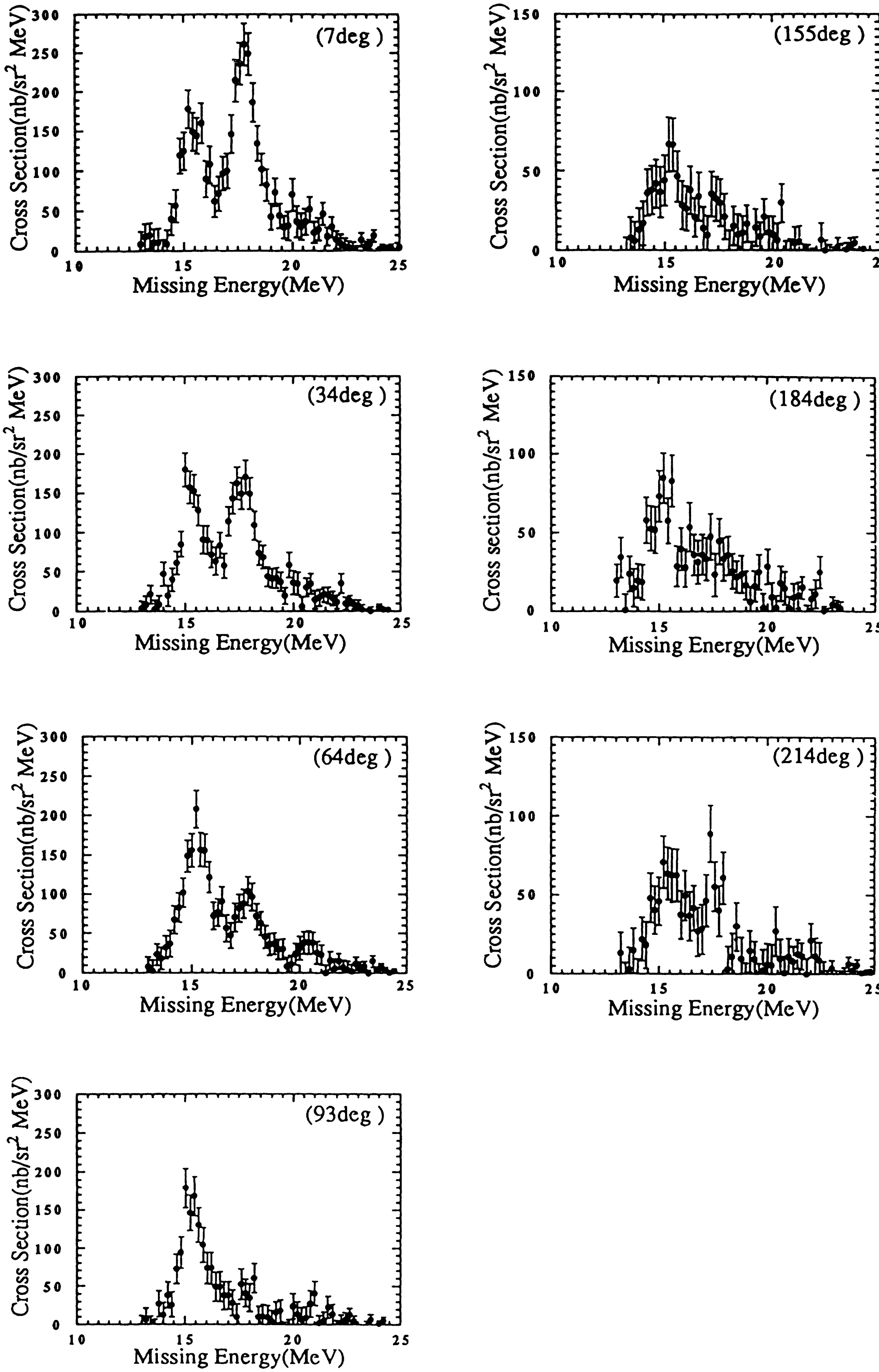

FIG. 5. Missing energy spectra for the ^{40}Ca$(e, e'n)^{39}$Ca reaction. The peak at 15.6 MeV corresponds to the neutrons feeding the ground state in ^{39}Ca and the peak at 17.8 MeV corresponds to the neutrons feeding the first, second, and third excited states in ^{39}Ca.

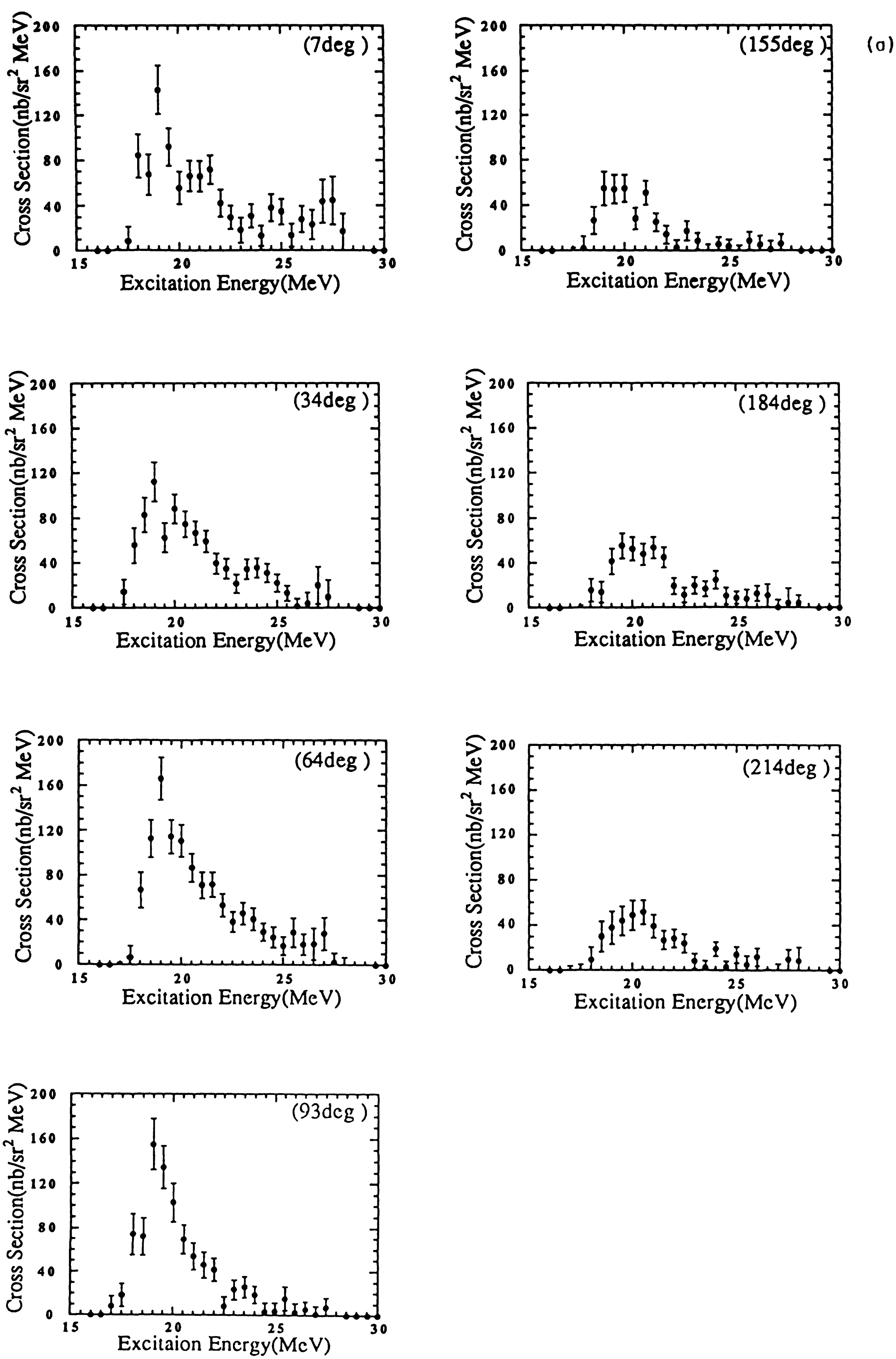

FIG. 6. Differential cross sections for the reactions (a) ^{40}Ca$(e, e'n_0)^{39}$Ca and (b) ^{40}Ca$(e, e'n_1)^{39}$Ca.

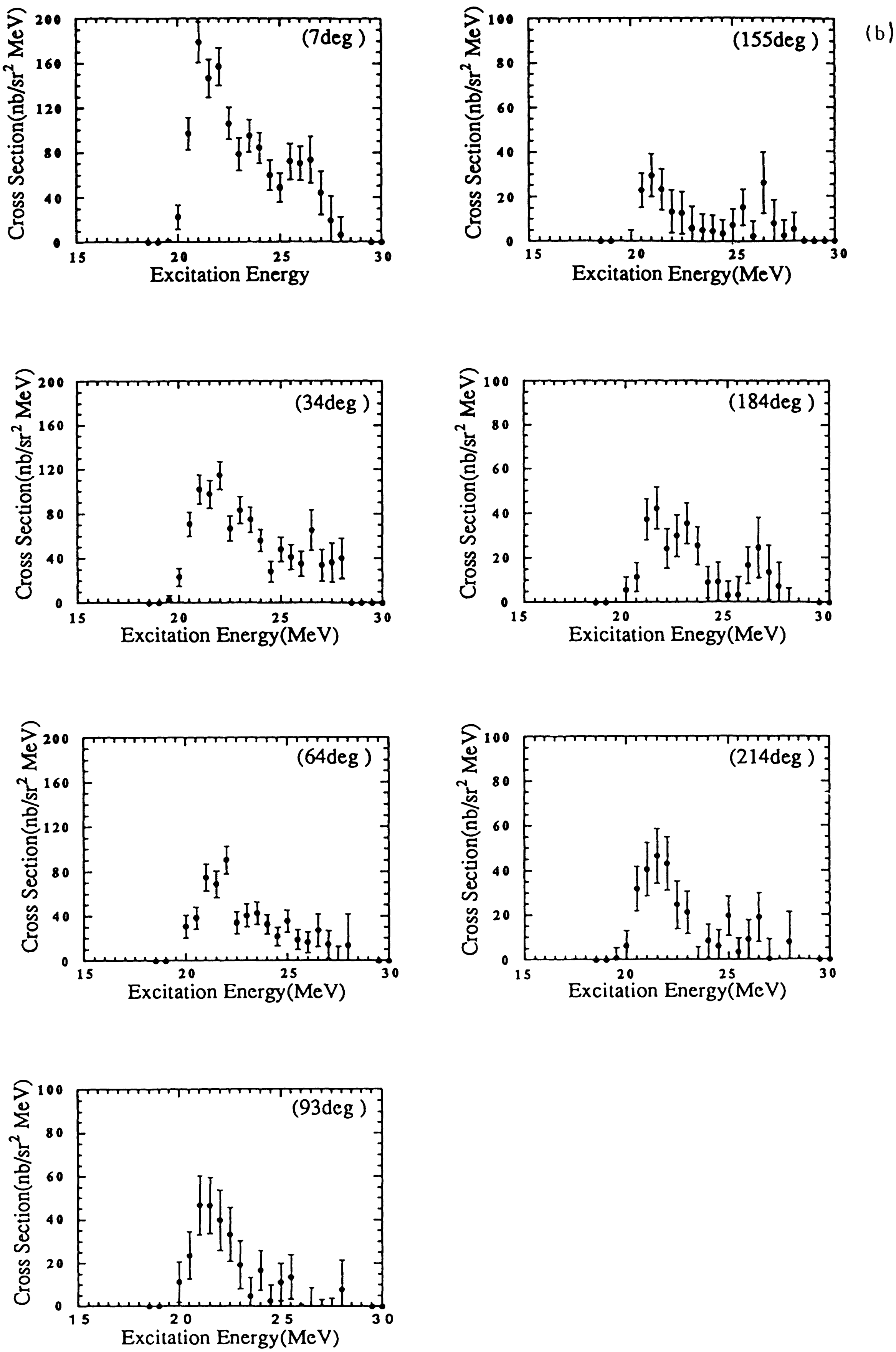

FIG. 6. (Continued).

TABLE I. Differential cross sections (nb/sr^2 MeV) for the ^{40}Ca$(e,e'n_0)^{39}$Ca reaction.

Angles	19 MeV	20 MeV	21 MeV	22 MeV	23 MeV	24 MeV	25 MeV	26 MeV	27 MeV
7°	235 ± 28	122 ± 22	138 ± 19	72 ± 18	49 ± 15	51 ± 14	48 ± 16	51 ± 16	68 ± 23
34°	176 ± 23	164 ± 18	127 ± 16	75 ± 13	57 ± 12	67 ± 12	36 ± 12	6 ± 10	14 ± 19
64°	281 ± 25	197 ± 21	142 ± 17	91 ± 15	87 ± 13	54 ± 13	46 ± 12	38 ± 16	22 ± 20
93°	290 ± 28	173 ± 26	100 ± 18	50 ± 16	50 ± 13	22 ± 12	20 ± 11	8 ± 14	13 ± 11
155°	109 ± 19	84 ± 17	77 ± 14	17 ± 11	26 ± 11	5 ± 10	4 ± 9	14 ± 9	11 ± 11
184°	96 ± 15	100 ± 15	98 ± 14	31 ± 12	36 ± 10	35 ± 10	17 ± 9	24 ± 11	15 ± 12
214°	82 ± 20	101 ± 18	66 ± 15	53 ± 11	12 ± 11	23 ± 9	20 ± 9	10 ± 11	8 ± 7

$$d^3\sigma/d\Omega_e\, d\omega\, d\Omega_n = \sigma_M\{V_L W_L + V_T W_T + V_{LT} W_{LT} \cos\phi_n + V_{TT} W_{TT} \cos 2\phi_n\} , \quad (1)$$

where σ_M is the Mott cross section for scattering on a point nucleus. The structure functions W_i contain all the nuclear structure information. They depend on the momentum transfer q, the energy transfer ω, the momentum k_x of the emitted nucleon, and the nucleon polar angle θ. The interference terms depend on the azimuthal angle ϕ. The leptonic kinematic factors V_i are expressed as

$$\begin{aligned} V_L &= q_\mu^4/q^4 , \\ V_T &= -q_\mu^2/(2q^2) + \tan^2\left(\frac{\theta_e}{2}\right) , \\ V_{LT} &= (k_i + k_f)\tan\left(\frac{\theta_e}{2}\right) q_\mu^2/q^3 , \\ V_{TT} &= -q_\mu^2/(2q^2) , \end{aligned} \quad (2)$$

where θ_e is the scattering angle of electron, k_i and k_f the momenta of incident and scattered electrons, respectively, and q_μ the four-momentum transfer.

Under the present experimental conditions of forward scattering ($\theta_e = 30°$), $q_{\rm eff} = 0.35$ fm^{-1}, the giant dipole resonance is mainly excited through longitudinal interaction (C_1); the transverse component (T_1) and other multipoles (C_2) may be weakly excited [20]. In this case, the longitudinal and transverse structure functions W_L and W_T can be expressed by $\mid C_1 \mid^2, C_1^* \cdot C_2$, and $\mid T_1 \mid^2$. The interference terms W_{LT} can be expressed by $C_1^* \cdot T_1$, $C_2^* \cdot T_1$, and W_{TT} by $\mid T_1 \mid^2$.

The transition matrix elements $C_1(q), C_2(q)$ and $T_1(q)$ are expressed as

$$\begin{aligned} C_1(q) &= \langle 1^- \mid\mid M_1(q) \mid\mid 0^+ \rangle , \\ C_2(q) &= \langle 2^+ \mid\mid M_2(q) \mid\mid 0^+ \rangle , \\ T_1(q) &= \langle 1^- \mid\mid T_1^{\rm el}(q) \mid\mid 0^+ \rangle, \end{aligned} \quad (3)$$

where $M_i(q)$ is the Coulomb multipole operators and $T_1^{\rm el}(q)$ is the transverse electric dipole operator.

The transverse matrix element can be estimated from the Coulomb matrix element [21] using the Goldhaber-Teller model [22] as

$$T_1(q) = -\sqrt{2}(\omega/q) C_1(q) . \quad (4)$$

This gives $T_1(q)/C_1(q) = -0.43$ under the present conditions of $\omega = 21$ MeV and $q_{\rm eff} = 0.35$ fm^{-1}. The ratio of transverse excitation cross section to the longitudinal cross section is expressed as

$$\delta = (V_T/V_L)[T_1(q)/C_1(q)]^2 , \quad (5)$$

which gives 0.118 for the present conditions.

C. Angular distribution

Experimental angular distributions for the $(e,e'n_0)$ and $(e,e'n_1)$ reactions on ^{40}Ca are summarized in Tables I and II. These angular distributions were fitted with the following Legendre parameters. The present structure functions are approximated by a series of Legendre polynomials and associated Legendre polynomials up to third order:

$$\begin{aligned} V_L W_L + V_T W_T &= A_0[1 + b_1 P_1(x_n) + b_2 P_2(x_n) \\ &\quad + b_3 P_3(x_n)] , \\ V_{LT} W_{LT} &= C_2[c_1 P_1^1(x_n) + P_2^1(x_n) + c_3 P_3^1(x_n)] , \\ V_{TT} W_{TT} &= D_2 P_2^2(x_n) , \\ x_n &= \cos\theta_n . \end{aligned} \quad (6)$$

TABLE II. Differential cross sections (nb/sr^2 MeV) for the ^{40}Ca$(e,e'n_1)^{39}$Ca reaction.

Angles	21 MeV	22 MeV	23 MeV	24 MeV	25 MeV	26 MeV	27 MeV
7°	277 ± 23	304 ± 24	186 ± 21	180 ± 20	109 ± 19	143 ± 22	118 ± 29
34°	173 ± 17	212 ± 18	151 ± 16	131 ± 15	76 ± 14	76 ± 16	100 ± 23
64°	113 ± 16	159 ± 17	75 ± 15	76 ± 13	57 ± 13	36 ± 13	42 ± 19
93°	71 ± 17	87 ± 19	53 ± 17	21 ± 13	14 ± 12	7 ± 13	0 ± 17
155°	53 ± 12	37 ± 13	19 ± 14	10 ± 10	11 ± 10	18 ± 11	34 ± 17
184°	48 ± 11	66 ± 13	65 ± 13	34 ± 11	12 ± 11	20 ± 11	37 ± 18
214°	72 ± 15	89 ± 17	46 ± 14	7 ± 10	26 ± 11	13 ± 11	19 ± 14

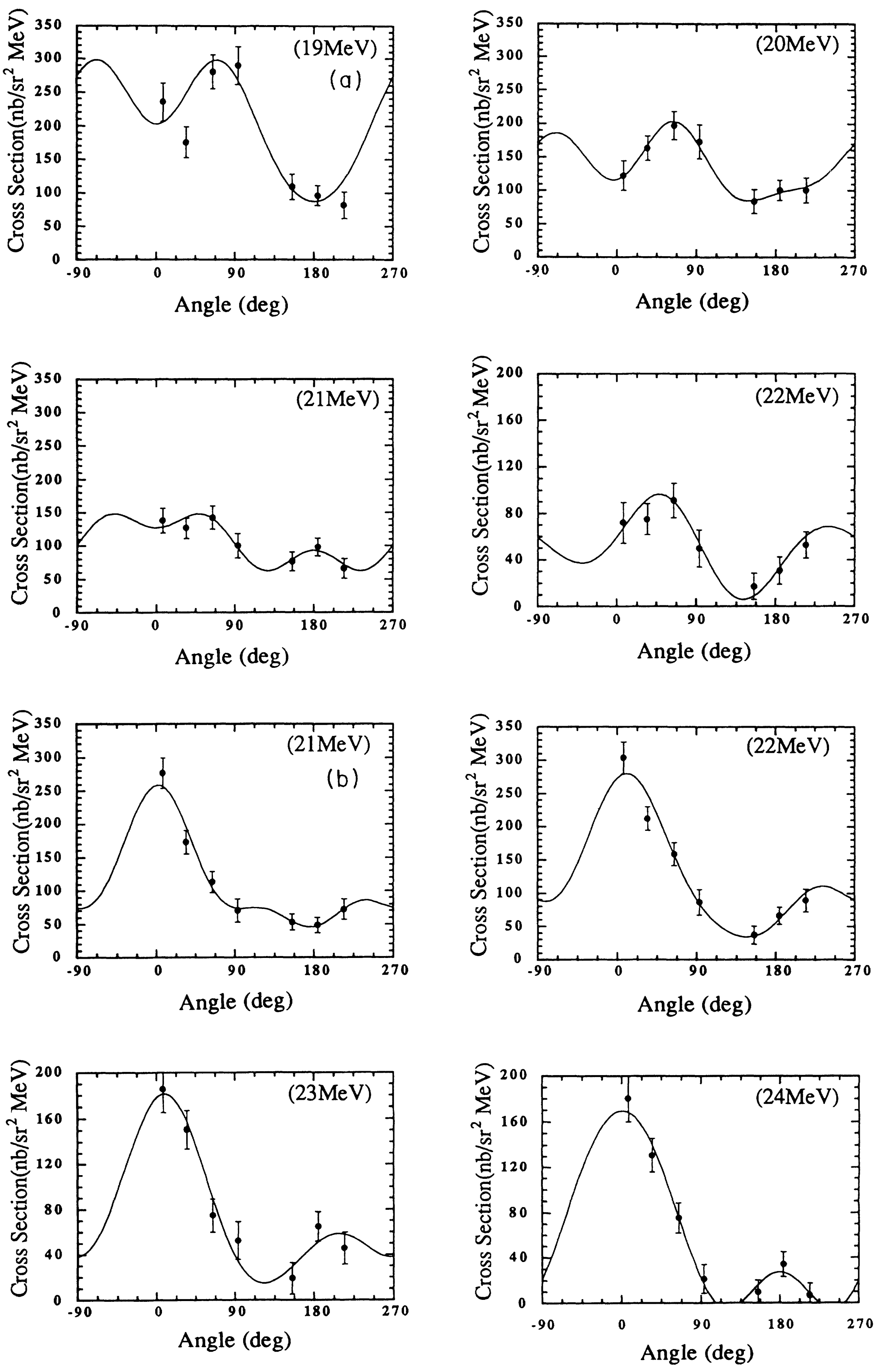

FIG. 7. Angular distributions of neutrons measured in the reactions (a) $^{40}Ca(e,e'n_0)^{39}Ca$ and (b) $^{40}Ca(e,e'n_1)^{39}Ca$. The excitation energy range is indicated. Solid lines represent Legendre polynomial fits with Eq. (6).

The $V_{TT}W_{TT}$ term was neglected in this analysis, since $V_{TT}W_{TT}$ is less than $V_T W_T$ in general [23,24]. The interference terms $c_1 P_1^1(x_n)$ and $c_3 P_3^1(x_n)$ were also neglected. These terms are assumed to be less than the main longitudinal-transverse interference term $C_2 P_2^1(x_n)$, because they involve interference between $E1$ and $E2$, and the longitudinal and transverse excitation modes. Five parameters, A_0, b_1, b_2, b_3, and C_2 were used in the fitting. The experimental angular distributions for each excitation energy region were χ^2 fitted with Eq. (6) and the Legendre polynomial coefficients were obtained. Figures 7(a) and 7(b) show typical angular distributions of the $(e,e'n_0)$ and $(e,e'n_1)$ reactions on ^{40}Ca with the fitted curves.

IV. DISCUSSION

A. Comparing with $(e,e'p)$ reaction

Figure 8 shows the b_1, b_2, b_3 parameters in the energy range of 19–25 MeV for the ${}^{40}\mathrm{Ca}(e,e'n_0){}^{39}\mathrm{Ca}$ reaction together with those in the energy range of 17.5 MeV to 21 MeV for the ${}^{40}\mathrm{Ca}(e,e'p_0){}^{39}\mathrm{K}$ reaction [13]. Comparing these parameters for both reactions we note that the values of b_1 for the two reactions are very similar and vary smoothly from -0.5 at 17.5 MeV to 0.5 at 20 MeV. The parameter b_2 which involves $E1$ and/or $E2$ amplitudes is different in the energy range of 19–21 MeV: the b_2 parameter for $(e,e'n_0)$ averages to -0.08 but for $(e,e'p_0)$ its value is about 0.8. This difference in angular distributions for protons and neutrons may indicate the interference between the $T=0$ quadrupole resonance and the $T=1$ giant dipole resonance, as suggested by Cavinato *et al.* [14].

The nonzero values of the b_1 and b_3 also indicate interference between dipole and quadrupole excitation, probably the GQR. The charged particle decay of the GQR at 18 MeV was confirmed by inelastic hadron scattering [6–11]. The parameter b_3 for the two reactions, has roughly opposite trend to b_1, decreasing with excitation energy. There is a significant difference around ~ 21 MeV in the value of b_3 for the two reactions.

The corresponding parameters b_1, b_2, and b_3 for the reactions ${}^{40}\mathrm{Ca}(e,e'n_1){}^{39}\mathrm{Ca}$ and ${}^{40}\mathrm{Ca}(e,e'p_1){}^{39}\mathrm{K}$ are shown in Fig. 9. In both cases the data are the coefficients for

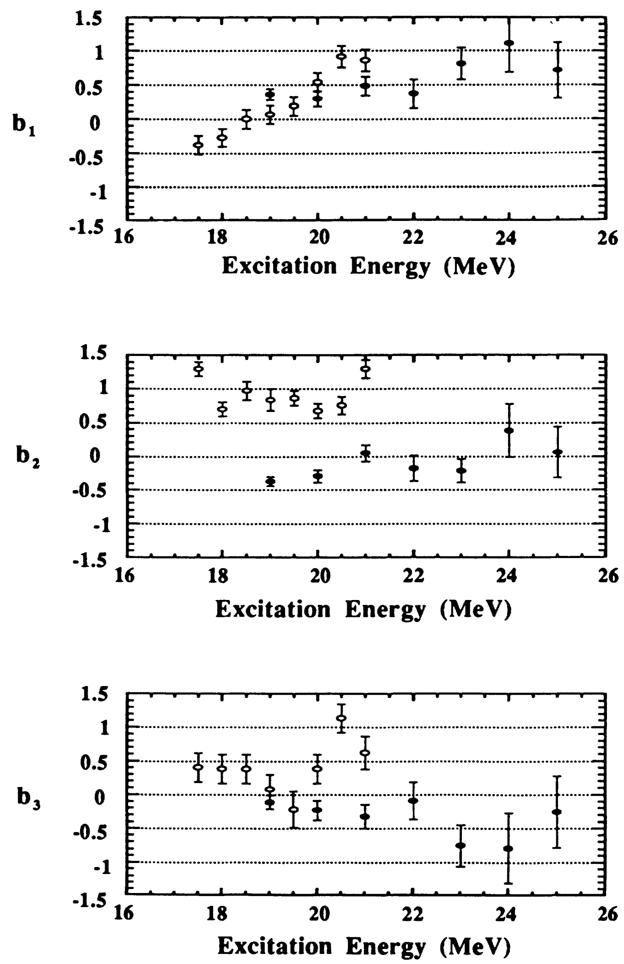

FIG. 8. The angular coefficients b_1, b_2, b_3 obtained by a fit of the Legendre expansion for the ${}^{40}\mathrm{Ca}(e,e'n_0){}^{39}\mathrm{Ca}$ reaction (solid circles). The results of the present experiment are compared with those for the ${}^{40}\mathrm{Ca}(e,e'p_0){}^{39}\mathrm{K}$ reaction of Tanaka *et al.* [13] (open circles).

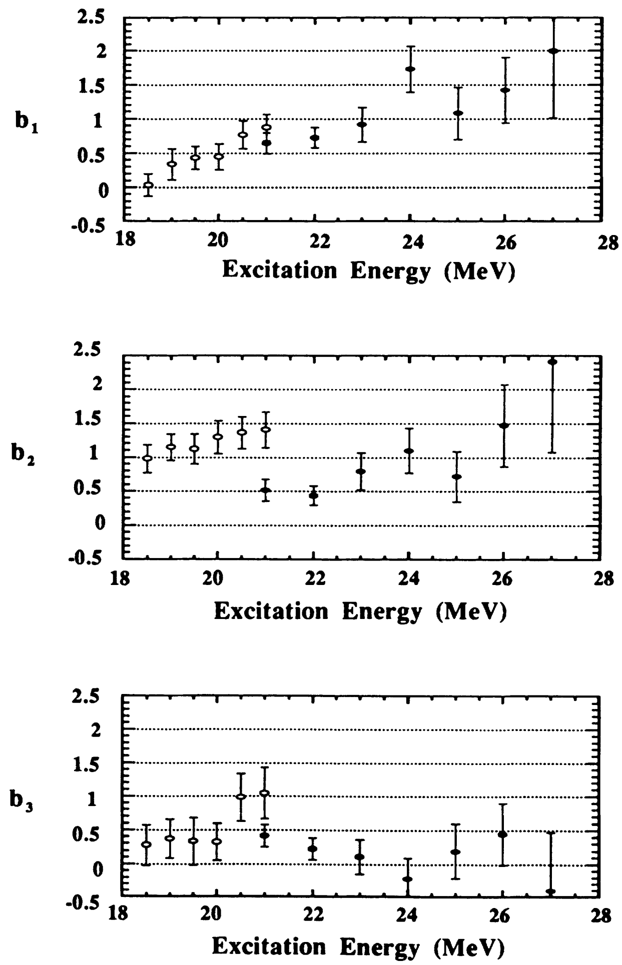

FIG. 9. The angular coefficients b_1, b_2, b_3 obtained by a fit of the Legendre expansion for the ${}^{40}\mathrm{Ca}(e,e'n_1){}^{39}\mathrm{Ca}$ reaction (solid circles). The results of the present experiment are compared with those for the ${}^{40}\mathrm{Ca}(e,e'p_1){}^{39}\mathrm{K}$ reaction of Tanaka *et al.* [13] (open circles).

the sum of the cross sections for the first three excited states, since they could not be experimentally resolved. The measured regions for p_1 and n_1 are different except for the data at $\omega = 21$ MeV.

The parameter b_1 for both $(e,e'n_1)$ and $(e,e'p_1)$ is similar and tends to increase with the excitation energy. The parameter b_3 is 0–0.5 for both $(e,e'n_1)$ and $(e,e'p_1)$. But the parameter b_2 behaves differently for $(e,e'n_1)$ and $(e,e'p_1)$. At an excitation energy 21 MeV, the value of b_2 is 0.5 for $(e,e'n_1)$ but for $(e,e'p_1)b_2$ is much larger at 1.4. Comparing $(e,e'n_0)$ with $(e,e'n_1)$ the differences in the angular distribution are reflected in each parameter. A large forward-backward asymmetry for the $(e,e'n_1)$ reaction suggests the presence of $E1$-$E2$ interference in the $(e,e'n_1)$ reaction, where the parameters b_1 and b_3 are about twice as large as those of $(e,e'n_0)$.

B. Comparing with (γ, n_0)

The $(e,e'n_0)$ cross section is closely related to that of (γ,n_0). The $(e,e'n_0)$ cross section measured at $q_{\text{eff}} = 0.35\ \text{fm}^{-1}$ was reduced to provide a value at photon point $(q=\omega)$, and was compared with the (γ,n_0) cross section. According to Kleppinger and Walecka [23], on the assumption of the static-limit resonance approximation, the longitudinal, transverse, and longitudinal-transverse structure functions are given by

$$\begin{aligned} W_L &= D \mid C_1(q) \mid^2 [1 + d_1P_1(x_n) + d_2P_2(x_n) \\ &\quad + d_3P_3(x_n)] \ , \\ W_T &= D \mid T_1(q) \mid^2 [1 - (1/2)d_2P_2(x_n)] \ , \\ W_{LT} &= D \cdot (d_2/\sqrt{2})\text{Re}(C_1(q)^*T_1(q))[c_1P_1^1(x_n) \\ &\quad + P_2^1(x_n) + c_3P_3^1(x_n)] \ , \\ D &\equiv Br/Z^2 \ , \end{aligned} \tag{7}$$

where Br is the branching ratio for n_0 and n_1 decays from the resonance state. In this analysis, parameters c_1 and c_3 were neglected for the reason mentioned previously. Using Eqs. (6) and (7), the Legendre polynomial coefficients are expressed by

$$\begin{aligned} A_0 &= D[V_L \mid C_1(q) \mid^2 + V_T \mid T_1(q) \mid^2] \\ &= DV_L \mid C_1(q) \mid^2 (1+\delta) \ , \\ b_1 &= d_1/(1+\delta), \\ b_2 &= d_2[1-(1/2)\delta]/(1+\delta) \ , \\ b_3 &= d_3/(1+\delta) \ , \\ C_2 &= D\, V_{LT}\sqrt{(1/2)}d_2\text{Re}(C_1(q)^*T_1(q)) \ . \end{aligned} \tag{8}$$

In the analysis of $^{40}\text{Ca}(e,e'p_0)^{39}\text{K}$, Tanaka et al. did a fit to the data which included the parameters c_1 and c_3. They found that the coefficients were nearly zero above 18.5 MeV.

On the other hand, the photoreaction cross section is expressed by

$$\begin{aligned} \frac{d\sigma}{d\Omega} &= \frac{2\pi^2\alpha}{\omega}3Br \mid T_1(\omega) \mid^2 [1 + a_1P_1(x_n) \\ &\quad + a_2P_2(x_n) + a_3P_3(x_n)] \ . \end{aligned} \tag{9}$$

The angular coefficients a_i are related to the coefficients d_i of the $(e,e'n_0)$ reaction by the following equation [13]:

$$\begin{aligned} d_1 &= \tfrac{4}{3}(q/\omega)a_1 \ , \\ d_2 &= -2a_2 \ , \\ d_3 &= -2(q/\omega)a_3 \ . \end{aligned} \tag{10}$$

In deriving these equations, the Siegert relation at the photon point, and the $j_1(qR)$ and $j_2(qR)$ dependence [25] of the longitudinal form factors of the GDR and GQR, were assumed.

The Legendre polynomial coefficients a_i derived from the $^{40}\text{Ca}(e,e'n_0)^{39}\text{Ca}$ data, after transformation using Eqs. (8) and (10), are compared with a_i taken from the (γ,n_0) data [4] in Fig. 10. The coefficients a_2 which value is different in the $(e,e'n_0)$ and $(e,e'p_0)$ reactions,

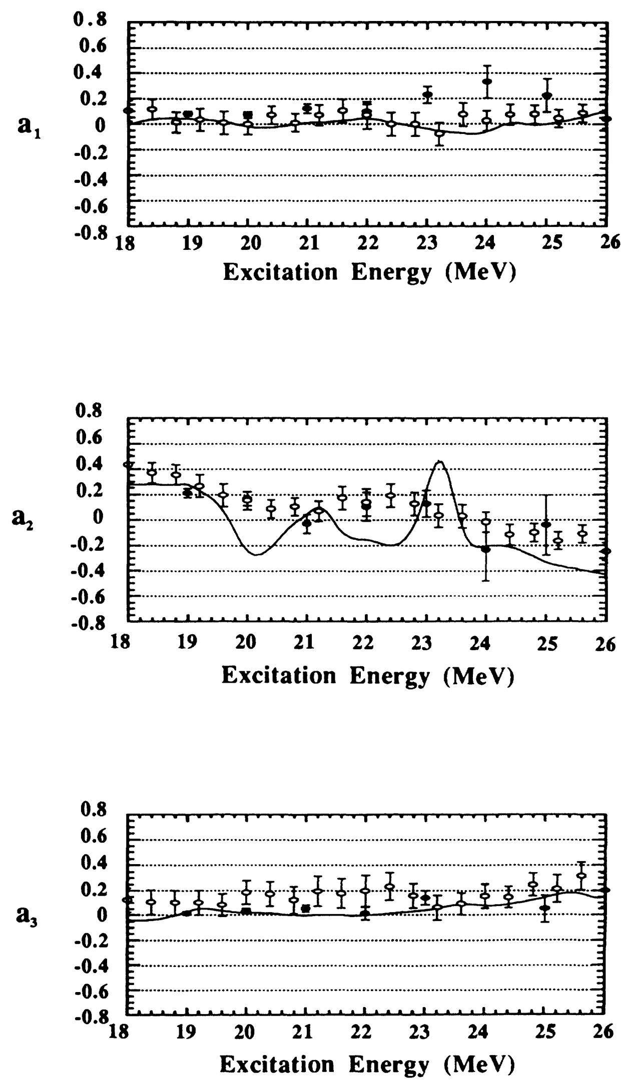

FIG. 10. The angular coefficients a_1, a_2, a_3 transformed from the coefficients b_1, b_2, b_3 for the reaction $^{40}\text{Ca}(e,e'n_0)^{39}\text{Ca}$ (solid circles) are compared with those for the reaction $^{40}\text{Ca}(\gamma,n_0)^{39}\text{Ca}$ of Kellie et al. [4] (open circles) and an RPA calculation of Cavinato et al. [5] (solid lines).

changes from 0.2 at $\omega = 19$ MeV to a small value as the excitation energy increases, and becomes negative above $\omega = 24$ MeV. The coefficient a_2 of $(e,e'n_0)$ is consistent with that of (γ,n_0). Both a_1 and a_3 which express $E1$-$E2$ interference terms are similar in the $(e,e'n_0)$ and (γ,n_0) reactions. This result indicates $E1$-$E2$ interference effects in the $(e,e'n_0)$ and (γ,n_0) reactions might be similar.

Recently Cavinato *et al.* [5] calculated the angular distribution for the $^{40}Ca(\gamma,n_0)^{39}Ca$ reaction within the framework of a self-consistent continuum RPA theory with a Skyrme force. Their calculation for photon energies ranging from 17 to 30 MeV is shown by the solid line in Fig. 10. There is agreement both in magnitude and shape between the experimental and theoretical values for the a_1 and a_3 coefficients. For the a_2 coefficient the general trend of the experimental points is similar to the RPA calculation, but the RPA calculation shows considerable structure. For ^{40}Ca, most of the $E1$ strength is located between 15 and 25 MeV. The RPA calculation, with a $1p$-$1h$ configuration shows $T = 1$, $E1$ strength at excitation energies of 17.6, 19.5, 20.3, and 22.3 MeV. The interference effects associated with the presence of these configurations are responsible for the structure in the calculated a_2. If the calculation were extended to include spreading of the $1p$-$1h$ states into complex configurations such as $2p$-$2h$ states, the Legendre polynomial coefficients are expected to average out and agree better with the experimental values.

Tanaka *et al.* [13] compared the angular coefficients of $(e,e'p_0)$ with that of (p,γ_0) which is the inverse reaction of (γ,p_0) [26], and found that they were in good agreement. Since we have observed the $(e,e'n_0)$ and (γ,n_0) angular distributions to be similar also, it is reasonable to conclude that there is no difference between the photoreaction and the corresponding $(e,e'x)$ reaction in the present energy and momentum transfer region. According to Cavinato *et al.* [5], the angular distributions calculated for (γ,n_0) and (γ,p_0) reactions below excitation energy 22 MeV, as specified by a_2, are different. As mentioned in Sec. IV A, coefficients b_2 obtained from the experiments are also different for $(e,e'n_0)$ and $(e,e'p_0)$. Since in both types of reactions the angular distribution depends markedly on whether a proton or a neutron is emitted, we conclude that the isospin involved in the reaction plays an important role in the angular distribution.

C. Longitudinal-transverse interference term

The longitudinal-transverse term $\mathrm{Re}\{C_1(q)^* \cdot T_1(q)\}$ is a characteristic of coincidence experiments and gives the phase difference between longitudinal and transverse transitions. Figure 11 shows the coefficient C_2 which gives the phase difference between the L-T terms for $(e,e'n_0)$ and $(e,e'p_0)$. In analyzing the $(e,e'n)$ reaction, we considered the L-T term, but not the interference between L-T and $E1$-$E2$ interference, but in analyzing the $(e,e'p)$ reaction Tanaka *et al.* did not make this simplification. This difference may appear in the coefficient

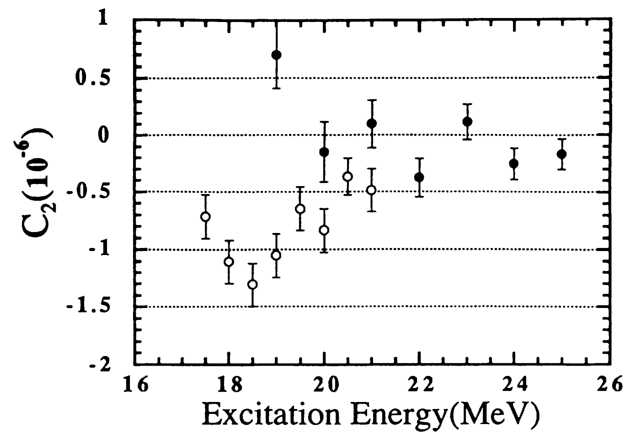

FIG. 11. Longitudinal-transverse interference term for the $^{40}Ca(e,e'n_0)^{39}Ca$ reaction (solid circles) is compared with the $^{40}Ca(e,e'p_0)^{39}K$ reaction of Tanaka *et al.* [13] (open circles).

C_2 for the $(e,e'n_0)$ reaction, which is 0.7 at 19 MeV. If Siegert theorem holds, the L-T term must be negative, but in the case it shows positive. However, the data at 19 MeV is near detection threshold where the yield is critical for fluctuations in the detection threshold and efficiency correction for low-energy neutrons. The data may have a larger systematic error than that of other experimental points.

Figure 12 shows the coefficient C_2 for the $(e,e'n_1)$ and $(e,e'p_1)$ reactions. In comparing them, the L-T term of $(e,e'n_1)$ is almost zero for the 24 MeV region but that of $(e,e'p_1)$ is nearly -1 for the 19 MeV region. However, both L-T terms seem to increase smoothly with excitation energy between 18.5 and 24 MeV. The difference in the L-T term for $(e,e'n_1)$ and $(e,e'p_1)$ might be due to the reaction mechanism, or to the difference in excitation energy. This difference may as well be due to different contributions between the neutron (n_2,n_3) and proton (p_2,p_3) decay. It is therefore important to compare the resolved $(e,e'n_1)$ and $(e,e'p_1)$ reactions in the same excitation energy region.

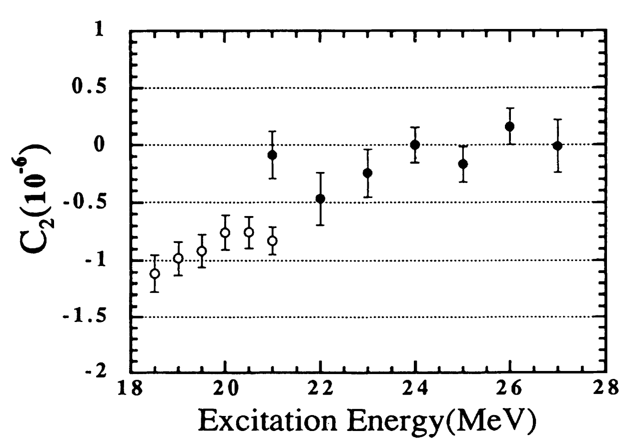

FIG. 12. Longitudinal-transverse interference term for the $^{40}Ca(e,e'n_1)^{39}Ca$ reaction (solid circles) is compared with the $^{40}Ca(e,e'p_1)^{39}K$ reaction of Tanaka *et al.* [13] (open circles).

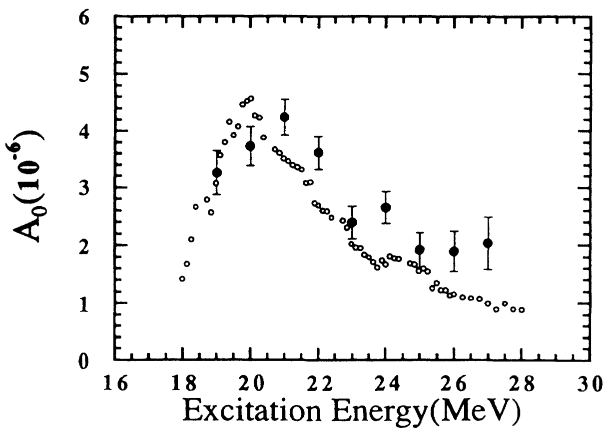

FIG. 13. ^{40}Ca$(e,e'n)^{39}$Ca longitudinal and transverse cross section measured in the present work (solid circles) in comparison with the values transformed from the photoabsorption cross section of Bezić et al. [27] and the branching ratio of the neutron decay (open circles). The cross sections are presented as ratios to the Mott cross section.

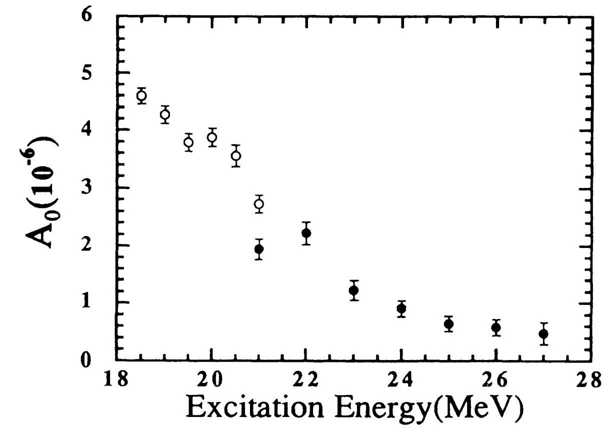

FIG. 15. ^{40}Ca$(e,e'n_1)^{39}$Ca longitudinal and transverse cross section measured in the present work (solid circles) in comparison with that for the reaction ^{40}Ca$(e,e'p_1)^{39}$K of Tanaka et al. [13] (open circles). Same units as Fig. 13.

D. Cross section

The total longitudinal and transverse cross sections obtained by A_0 multiplied by 4π is shown in Fig. 13. The cross section is presented as a ratio to the Mott cross section. In the figure it is compared with the data transformed from the photoreaction by the following method. Using the Siegert theorem, the transverse transition matrix element $| T_1(\omega) |^2$ from the photoabsorption data [27] is transformed to the longitudinal transition matrix element $| C_1(\omega) |^2$ at the photon point. Then assuming the Goldhaber Teller model, $| C_1(q) |^2$ at $q_{\rm eff} = 0.35$ fm^{-1} is estimated using the form factor of the Überall model [28]. The experimental branching ratio $R_{\rm Br} = \sigma(\gamma,n)/\sigma(\gamma,{\rm abs})$ was used.

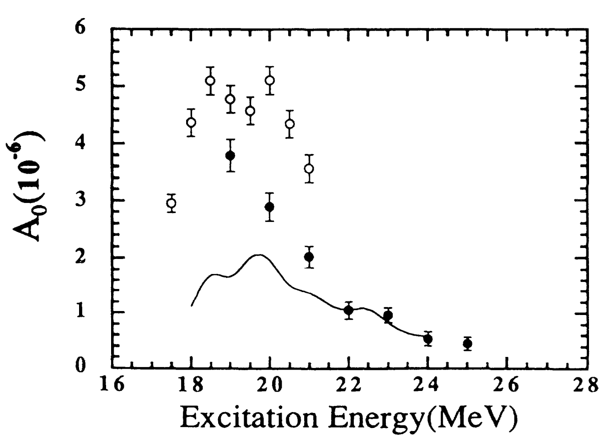

FIG. 14. ^{40}Ca$(e,e'n_0)^{39}$Ca longitudinal and transverse cross section measured in the present work (solid circles) in comparison with that for the reaction ^{40}Ca$(e,e'p_0)^{39}$K of Tanaka et al. [13] (open circles) and the values transformed from the reaction ^{40}Ca$(\gamma,n_0)^{39}$Ca of Kellie et al. [4] (solid line). Same units as Fig. 13.

From Fig. 13 it can be seen that the cross sections are in reasonable agreement. In the $(e,e'n)$ reaction the peak of the cross section is at about 21 MeV, but in the (γ,n) reaction the peak is at about 20 MeV. This may be because the neutron-detector threshold was 3 MeV and n_1 events might not be measured at $\omega = 20$ MeV.

The longitudinal and transverse cross sections for the $(e,e'n_0)$ and $(e,e'n_1)$ reactions are shown in Figs. 14 and 15. In Fig. 14, the $(e,e'n_0)$ cross section is in agreement with that of (γ,n_0) above an excitation energy of 22 MeV, but below 22 MeV it is larger than that of (γ,n_0). The large value at 19 MeV may be due to the simplification in fitting. According to Wu et al. [29], the ratio of $\sigma(\gamma,p_0)/\sigma(\gamma,n_0)$ is about 2.2. For the $(e,e'x)$ reaction, the ratio of $\sigma(e,e'p_0)/\sigma(e,e'n_0)$ is about 2 except near 19 MeV as shown in Fig. 14. For the $(e,e'n_1)$ cross section there is only one overlapping point with the $(e,e'p_1)$ data and there are no (γ,n_1) data to compare with. However, both cross sections are consistent in that they decrease smoothly with excitation energy.

V. CONCLUSION

The giant resonances in ^{40}Ca have been studied by measurements of the angular distributions and cross sections of decay neutrons from the ^{40}Ca$(e,e'n)^{39}$Ca reaction. The cross sections and angular distributions for n_0 and n_1 decays were obtained for the excitation energies between 19 and 27 MeV, at an effective momentum transfer of 0.35 fm^{-1}. The Legendre polynomial coefficients obtained from the data are compared with those from the $(e,e'p)$ and photoreaction data.

In comparing with the $(e,e'p_0)$ reaction, the interference coefficients b_1 and b_3 are in agreement with each other, but the noninterference coefficient b_2 is different in the energy range 19–21 MeV. The different behavior of the angular distributions for protons and neutrons may suggest the interference between a $T = 0$ quadrupole resonance and the $T = 1$ giant dipole resonance. A similar tendency was seen in the comparing with the $(e, e'p_1)$ reaction. The existence of the quadrupole resonance was also indicated in the nonzero values of the b_1 and b_3 coefficients.

The angular coefficients a_i transformed from the data agree well with those of the (γ, n) reaction. This supports the evidence of isoscalar $E2$ strength below 27 MeV as pointed out by Kellie *et al.*. The reduced total cross section is consistent for the $(e, e'n)$ and (γ, n) reactions, but the cross section for $(e, e'n_0)$ is larger than that of (γ, n_0) near the peak of the resonance. The longitudinal-transverse interference term was measured in the energy region of 19–25 MeV. The values for this term tend to zero, which is small compared with data near the peak of resonance, obtained from the $(e, e'p)$ reaction.

In comparing with hadron scattering, the isoscalar $T = 0$ quadrupole resonance in the energy range 19–21 MeV predicted in this experiment is consistent with the $T = 0$, GQR around $E_x = 18$ MeV observed in hadron scattering. Indication of weak $E2$ strength below 27 MeV does not contradict with an unexhausted energy-weighted-sum rule value for the region $E_x \leq 20$ MeV observed in hadron scattering.

ACKNOWLEDGMENTS

The authors would like to acknowledge Professor M. Sugawara for stimulating discussion, and Professor M. N. Thompson for a critical reading of the manuscript. We wish to thank Dr. O. Konno for his help during the experiment. We would like to thank the LINAC crew and staff of the Laboratory of Nuclear Science for providing the high quality beams.

[1] G. O. Bolme, L. S. Cardman, R. Doerfler, L. J. Koester, Jr., B. L. Miller, C. N. Papanicolas, H. Rothhaas, and S. E. Williamson, Phys. Rev. Lett. **61**, 1081 (1988).
[2] R. A. Miskimen *et al.*, Phys. Lett. B **236**, 251 (1990).
[3] S. Suzuki, T. Saito, K. Takahisa, C. Takakuwa, T. Tohei, T. Nakagawa, Y. Kobayashi, and K. Abe, Nucl. Instrum. Methods A **314**, 547 (1992).
[4] J. D. Kellie, A. R. Curran, S. J. Hall, G. I. Crawford, J. L. Robertson, and D. T. Burns, Nucl. Phys. **A515**, 125 (1990).
[5] M. Cavinato, M. Marangoni, and A. M. Saruis, Nucl. Phys. **A422**, 237 (1984).
[6] A. Moalem, W. Benenson, G. M. Crawley, and T. L. Khoo, Phys. Lett. **61B**, 167 (1976).
[7] A. Moalem, Nucl. Phys. **A281**, 461 (1977).
[8] D. H. Youngblood, A. D. Bacher, D. R. Brown, J. D. Bronson, J. M. Moss, and C. M. Rozsa, Phys. Rev. C **15**, 246 (1977).
[9] T. Yamagata *et al.*, Phys. Rev. Lett. **40**, 1628 (1978).
[10] F. Zwarts, K. van der Borg, A. G. Drentje, M. N. Harakeh, W. A. Sterrenburg, and A. van der Woude, Phys. Rev. C **25**, 2139 (1982).
[11] F. Zwarts, A. G. Drentje, M. N. Harakeh, and A. van der Woude, Phys. Lett. **125B**, 123 (1983); Nucl. Phys. **A439**, 117 (1985).
[12] S. Brandenburg, R. de Leo, A. G. Drentje, M. N. Harakeh, H. Sakai, and A. van der Woude, Phys. Lett. **130B**, 9 (1983).
[13] A. Tanaka, T. Hino, H. Kawahara, M. Nomura, T. Tamae, M. Sugawara, H. Tsubota, H. Miyase, and Y. Kawazoe, Nucl. Phys. **A489**, 381 (1988); A. Tanaka, Ph.D. thesis, Tohoku University, 1987.
[14] M. Cavinato, M. Marangoni, and A. M. Saruis, Phys. Lett. **163B**, 49 (1985); Phys. Rev. C **37**, 1823 (1988).
[15] T. Tamae *et al.*, Nucl. Instrum. Methods **A264**, 173 (1988).
[16] M. Kimura *et al.*, Nucl. Instrum. Methods **95**, 403 (1971).
[17] V. V. Verbinski, W. R. Burrus, T. A. Love, W. Zobel, N. W. Hill, and R. Textor, Nucl. Instrum. Methods **65**, 8 (1968).
[18] T. De Forest, Ann. Phys. (N.Y.) **45**, 365 (1967).
[19] M. Cavinato, D. Drechsel, E. Fein, M. Marangoni, and A. M. Saruis, Nucl. Phys. **A444**, 13 (1985).
[20] Y. Torizuka, K. Itoh, Y. M. Shin, Y. Kawazoe, H. Matsuzaki, and G. Takeda, Phys. Rev. C **11**, 1174 (1975).
[21] T. De Forest and J. D. Walecka, Adv. Phys. **15**, 1 (1966).
[22] M. Goldhaber and E. Teller, Phys. Rev. **74**, 1046 (1948).
[23] W. E. Kleppinger and J. D. Walecka, Ann. Phys. (N.Y.) **146**, 349 (1983).
[24] G. Co' and S. Krewald, Nucl. Phys. **A433**, 392 (1985).
[25] R. Helm, Phys. Rev. **104**, 1466 (1956).
[26] E. M. Diener, J. F. Amann, and P. Paul, Phys. Rev. C **7**, 695 (1973).
[27] N. Bezić, D. Jamnik, G. Kernel, J. Krajnik, and J. Šnajder, Nucl. Phys. **A117**, 124 (1968).
[28] H. Überall, Nuovo Cimento **41B**, 25 (1966).
[29] C.-P. Wu, J. E. E. Baglin, F. W. K. Firk, and T. W. Phillips, Phys. Lett. **29B**, 359 (1969).

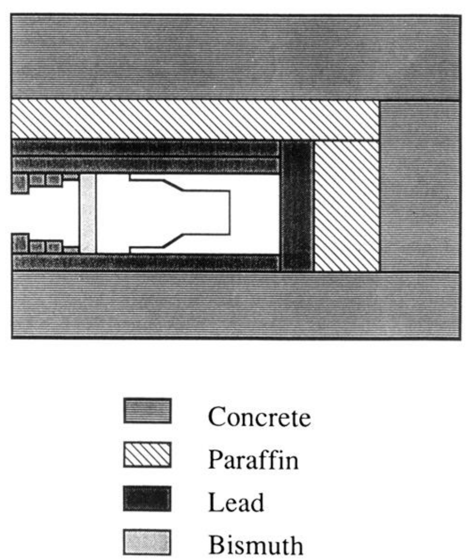

FIG. 2. Schematic view of the shielding for the neutron detectors.